

# MICROSTRUCTURE AND FATIGUE PROPERTIES OF CU–NI–SI ALLOY STRENGTHENED BY Ni<sub>2</sub>Si INTERMETALLIC COMPOUNDS

MASAHITO GOTO<sup>1</sup>, TAKAHITO UTSUNOMIYA<sup>1</sup>, TAKAEI YAMAMOTO<sup>1</sup>, SEUNG ZEON HAN<sup>2</sup>,  
JUNICHI KITAMURA<sup>1</sup>, JEE-HYUK AHN<sup>2</sup>, SUNG HWAN LIM<sup>3</sup> & TERUTOSHI YAKUSHIJI<sup>4</sup>

<sup>1</sup>Department of Mechanical Engineering, Oita University, Japan

<sup>2</sup>Korea Institute of Materials Science, Changwon, Republic of Korea

<sup>3</sup>Department of Advanced Materials Science and Engineering, Kangwon National University, Republic of Korea

<sup>4</sup>National Institute of Technology, Oita College, Japan

## ABSTRACT

Microstructure and fatigue properties of Cu–6Ni–1.5Si alloy having different morphologies of Ni<sub>2</sub>Si intermetallic compounds that are disk-shaped continuous precipitates (CPs) with nano-size diameter by normal aging, fibre-shaped discontinuous precipitates (DPs) by overaging and elongated DPs fabricated by cold-rolling (DPR) were studied. There was a negligible difference in fatigue strength between the CP and DP specimens despite higher tensile strength of the CP specimen. The DPR specimen had the highest tensile and fatigue strengths in all specimens. The fatigue crack initiation resistance of the DPR specimen was drastically enhanced. The growth rate of a small crack can be determined by a term  $\sigma_a^n l$ . The crack growth resistance of the DPR specimen was nearly equal to that of the CP specimen. The reason for such trends of tensile and fatigue strengths was discussed based on the microstructure of each specimen.

*Keywords: fatigue, copper alloy, crack initiation, microstructure, cold-rolling.*

## 1 INTRODUCTION

Cu–Ni–Si alloys [1] used for lead frame, connector applications are commercially manufactured through normal aging after solution heat treatment (SHT). Normal aging of Cu–6Ni–1.5Si alloy produced continuous precipitates (CPs) of nano-sized,  $\delta$ -Ni<sub>2</sub>Si intermetallic compounds which brought a high tensile strength throughout the matrix [1]–[4]. It is well known that an enhancement in the tensile strength of normal aged Cu alloys is inevitably accompanied by a reduction in electrical conductivity. On the other hand, overaging of Cu–Ni–Si alloys, particularly with high solute concentrations, produced discontinuous precipitates (DPs) that were fibre-shaped, stable  $\delta$ -Ni<sub>2</sub>Si intermetallic compounds in the Cu matrix. Mechanical properties of Cu–Ni–Si alloys are degraded by the formation of DPs [5]–[9], however DPs have a superior electrical conductivity. It has been shown that the DP specimen subjected to cold working had elongated nanofiber-shaped  $\delta$ -Ni<sub>2</sub>Si precipitates and the tensile strength was enhanced without a significant loss of electrical conductivity [8].

For the envisaged structural applications, fatigue strength should be clarified, because that at least 90% of mechanical failures during service were caused by the fatigue failure. To make the design and maintenance of safe machine components and structures, the fatigue behaviour such as crack initiation and propagation should be clarified. Up to now, there was a small number of studies [10]–[16] on fatigue behaviour of Cu–Ni–Si alloys, particularly in DPs. In the present study, fatigue tests of Cu–6Ni–1.5Si alloy with different morphologies of Ni<sub>2</sub>Si precipitates were carried out at the room temperature. The objective of this study is to investigate the microstructure and fatigue crack growth behaviour of Cu–Ni–Si alloy with different morphologies of Ni<sub>2</sub>Si precipitates.



For the envisaged structural applications, fatigue strength should be clarified, because that at least 90% of mechanical failures during service were caused by the fatigue failure. To make the design and maintenance of safe machine components and structures, the fatigue behaviour such as crack initiation and propagation should be clarified. Up to now, there was a small number of studies [10]–[16] on fatigue behaviour of Cu–Ni–Si alloys, particularly in DPs. In the present study, fatigue tests of Cu–6Ni–1.5Si alloy with different morphologies of  $\text{Ni}_2\text{Si}$  precipitates were carried out at the room temperature. The objective of this study is to investigate the microstructure and fatigue crack growth behaviour of Cu–Ni–Si alloy with different morphologies of  $\text{Ni}_2\text{Si}$  precipitates.

## 2 EXPERIMENTAL PROCEDURES

Using 99.9% pure Ni, and 99.99% pure Si as alloying elements, Cu–6wt%Ni–1.5wt%Si alloy was cast by induction melting. The cast was cold-rolled with 80% reduction in area, and subsequently solution heat-treated at 980°C for 1 h with water quenching. The solution heat-treated bars were aged at 500°C. The aging time was 0.5 and 3 h for CP and DP structure, respectively. In what follows, the specimen aged for 0.5 and 3 h is designated by the CP and DP specimen, respectively. Some of the cast were hot-rolled down to 75% reduction in area, and solution heat-treated at 980°C for 1 h. The solution heat-treated specimen was aged at 500°C for 3 h to obtain fully DP structure, then cold-rolled down to 80% reduction in area, which is designated as “DPR specimen”.

The microstructure was observed using an optical microscope (OM) and a scanning electron microscope (SEM). A 200 kV field-emission transmission electron microscope (TEM) was utilized to characterize precipitates. Disks 3 mm in diameter and 100- $\mu\text{m}$ -thick were prepared for the TEM observation by mechanical polishing with a digitally enhanced precision specimen grinder and dimpling by a dimple grinder. The microhardness ( $H_v$ ) was measured using a Vickers hardness tester with an applied load of 1 N. Tensile tests (4 mm diameter specimens) were performed on a tensile testing machine (4206, Instron) with a strain rate of 0.017  $\text{s}^{-1}$  at room temperature.

Fatigue specimens were round-bar with 5 mm diameter (Fig. 1) which machined from the CP, DP and DPR samples. To eliminate any surface damage induced during specimen preparation, the layer of approximately 25  $\mu\text{m}$  of the specimen's surface was removed by electrolytic polishing prior to fatigue testing. All fatigue tests were conducted at room temperature using a rotating bending fatigue machine (constant bending-moment type, the stress ratio:  $R = -1$ ) operating at 50 Hz. The observation of fatigue damage on the specimen surface and on the fracture surface was conducted using OM and SEM. The crack length,  $l$ , was measured along the circumferential direction of the surface using a plastic replication technique. The stress value referred to is that of the nominal stress amplitude,  $\sigma_a$ , at the minimum cross-section (5 mm diameter).

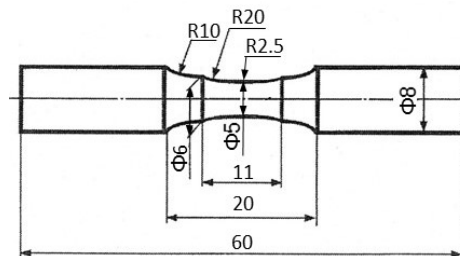


Figure 1: Schematic illustration of the fatigue specimen (in mm).

The electrical resistivity of a 300 mm length specimen was measured by a portable double bridge apparatus (2769, Yokogawa M&C) at room temperature ( $27 \pm 1^\circ\text{C}$ ). It was then converted to electrical conductivity by taking inverse of the resistance. The electrical conductivity was represented by the value of International Annealed Copper Standard (%IACS) which was calculated by the ratio of electrical conductivity between sample and annealed pure Cu.

### 3 EXPERIMENTAL RESULTS AND DISCUSSION

Fig. 2 shows OM micrograph of microstructure, Vickers hardness and electrical conductivity as a function of aging time. The hardness sharply increased with an increasing aging time. At 0.5 h aging, it reached near maximum value ( $H_v = 259$ ), followed by a gradual decreasing trend. The 0.5 h aged microstructure consisted of bright grains and sporadically distributed dark/tarnished phases. The dark phases were DPs. After 3 h aging, the matrix was transformed to fully DP phases (DP fraction was over 95%) and hardness dropped to 196. The electrical conductivity (%IACS) gradually increased with an increase in aging time. The conductivity for 0.5 h aging was 25%IACS. After 3 h aging, it was drastically enhanced to 44%IACS. Even though the formation of DPs was detrimental to the mechanical properties of Cu–Ni–Si alloys, the electrical conductivity of DPs was superior to that of the CP counterpart. The increased conductivity of DPs was caused by the further reduction of Ni and Si solute elements in the Cu matrix.

#### 3.1 Microstructure of the CP specimen

Fig. 3 shows the microstructure of the CP specimen. There were bright grains, dark/tarnished phases which sporadically distributed along grain boundaries (GBs) and inclusions with a

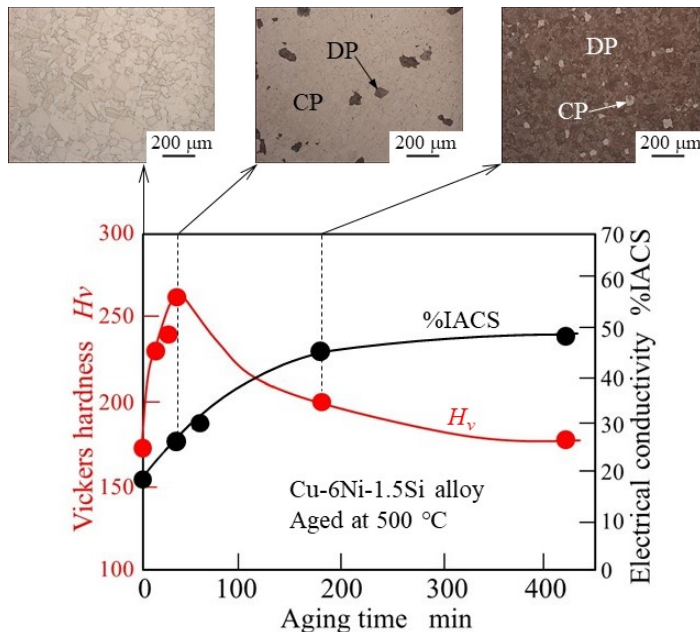


Figure 2: OM micrograph of microstructure, Vickers hardness and electrical conductivity as a function of aging time.

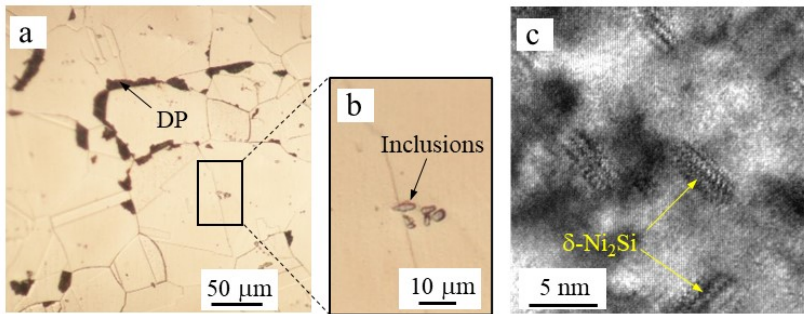


Figure 3: Microstructure of the CP specimen. (a), (b) OM micrograph; and (c) high-resolution TEM image of the matrix.

few micrometres in size (Fig. 3(a) and (b)). Fig. 3(c) shows high resolution TEM images of the matrix (bright grains in Fig. 3(a)). Disc-shaped precipitates with a few nanometres in diameter were observed. These precipitates were characterized as  $\delta\text{-Ni}_2\text{Si}$  intermetallic compounds by an optical diffractogram. As will be discussed in subsequent section, the dark phases in Fig. 3(a) were DPs with the fibre-shaped  $\text{Ni}_2\text{Si}$  precipitates which have also been called “cellular precipitates”.

Fig. 4(a) shows TEM images on the microstructure around GB areas in the CP specimen. A band-like bright zone and a particle with a few tens of nanometres were observed along the GBs (refer to magnified views: Fig. 4(b) and (d)). Fig. 4(c) and (e) indicated that the bright zone and particle was the precipitate-free zone (PFZ) and  $\text{NiSi}$  intrametric compounds (heterogeneous precipitates), respectively. Along with  $\text{NiSi}$ ,  $\text{Ni}_2\text{Si}$  intermetallics with a few tens of nanometres in size was also observed at GB areas [14]. The generation and subsequent growth of the heterogeneous precipitates ( $\text{NiSi}$ ,  $\text{Ni}_2\text{Si}$ ) at GBs were brought by the fast diffusion along the GBs. Accordingly, solute atoms’ absorption near the heterogeneous precipitates should lead to the formation of PFZ.

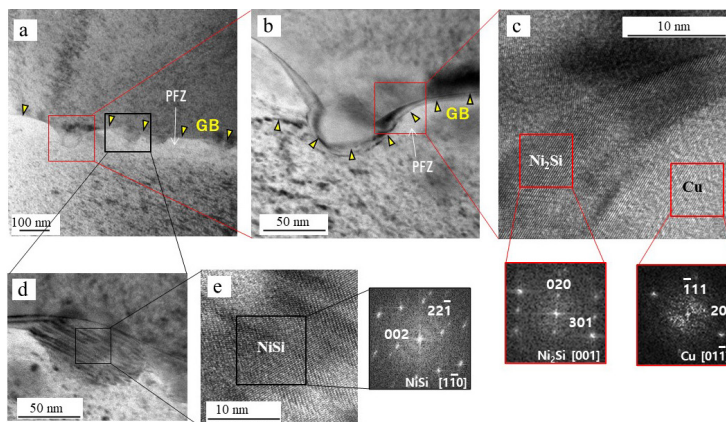


Figure 4: TEM micrographs of GB areas in the CP specimen.

### 3.2 Microstructure of the DP specimen

Fig. 5(a) shows the microstructure of the DP specimen, which consists of almost all DP phases. Inclusions with a few micrometres in size were formed and most of which were along GBs. The colonies of fibre-shaped  $\delta$ -Ni<sub>2</sub>Si intermetallic compounds were observed inside the grain [15]. Yellow arrow heads in Fig. 5(b) indicate the DP–DP–phase boundaries in the grain. It has been established that DP is formed by the decomposition of supersaturated solid solution into solute-depleted matrix and precipitates across moving boundary [17]. Previous study [15] on the formation of DP structure has shown that after DP generation at the GBs, the DPs grew toward the grain interior with moving boundaries. Colonies of Ni<sub>2</sub>Si fibre (Fig. 5(c)) with an extremely high aspect ratio were then formed within intergranular DPs. The DPs grew along a specific orientation in the Cu matrix, even though their growth orientations were not always uniform inside the same grain (parent grain). Although the formation of DPs is detrimental to the hardness of Cu–Ni–Si alloys, the electrical conductivity of DPs is superior to that of the normal aged alloy with the highest hardness (Fig. 2). The further reduction of Ni and Si solute elements in the Cu matrix during the DP formation induced the high electrical conductivity of DP specimen.

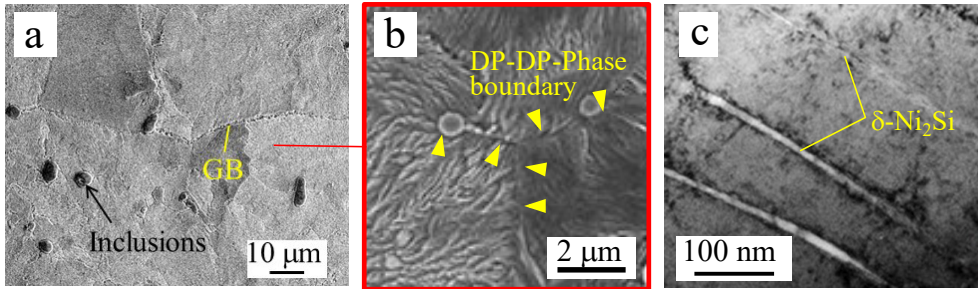


Figure 5: Microstructure of the DP specimen. (a) OM micrograph; (b) DP–DP–phase boundaries characterized by colonies of fibre-shaped Ni<sub>2</sub>Si with a specific orientation; and (c) TEM image of Ni<sub>2</sub>Si fibre in the Cu matrix.

### 3.3 Microstructure of the cold-rolled DP specimen

Simultaneous increase in electrical conductivity and tensile strength of precipitate strengthened Cu–Ni–Si alloys is often extremely difficult, because a decrease in electric conductivity is inevitably caused by the available strengthening mechanism. Using Cu–6Ni–1.4Si–0.1Ti alloys, Han et al. [8] fabricated alloys with fully DP phases through a prolonged aging (overaging) process. The product was then mechanically rolled with 90% reduction in area. Such a rolled DP phases showed a simultaneous increase in electrical conductivity and tensile strength by 1.3 times compared with conventional precipitate-strengthened Cu alloys. These recent results suggest that Cu alloys with fully DP phases processed by severe plastic deformation have a great potential as electrical materials with high electrical conductivity and super-high strength. Here, the microstructure of DP phases subjected to cold-rolling was investigated. Accordingly, some of the specimens with fully DP phases were then cold-rolled down to 80% reduction in area (DPR specimen).

Fig. 6(a) shows the OM micrograph observed on the surface of DP specimen. The DP phases were composed of fibre-shaped Ni<sub>2</sub>Si intrametric compound and Cu matrix (Fig. 6(c)).

Fig. 6(b) is the OM micrograph of the DPR specimen, showing stream lines along rolling direction. These lines were the array of  $\text{Ni}_2\text{Si}$  intermetallic fibres which tend to align along the direction of cold-rolling (Fig. 6(d)). The analysis [18] on the nanofiber in DP structure showed that the diameter of intermetallic fibre reduced from 14 to 7 nm as the result of 80% cold-rolling, while the average spacing between them reduced from 87 to 41 nm.

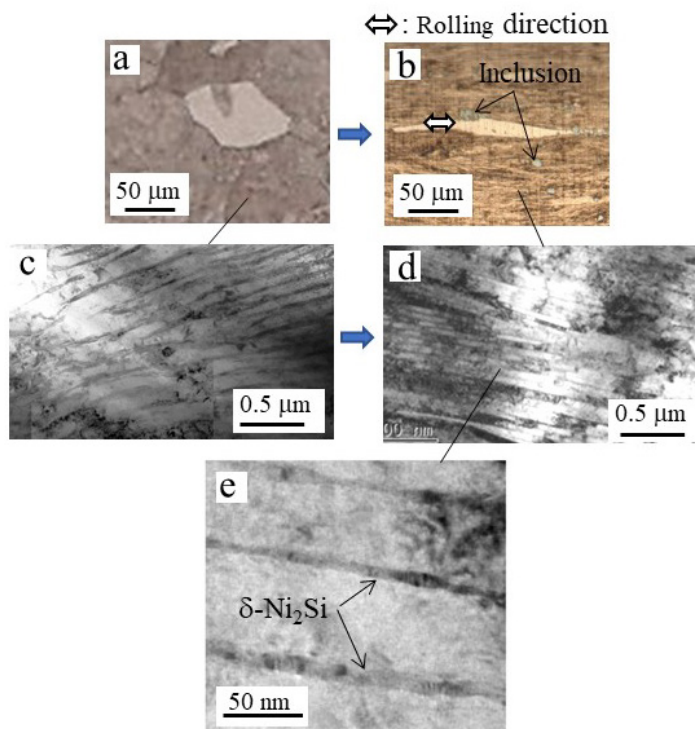


Figure 6: OM and TEM micrographs of the DPR specimen. (a) and (c) Microstructure before cold-rolling; (b) and (d) Microstructure after cold-rolling; and (e) Magnified view of  $\text{Ni}_2\text{Si}$  fibre after cold-rolling.

### 3.4 Tensile properties of precipitate strengthened Cu–6Ni–1.5Si alloy

The stress–strain curves of the CP, DP and DPR specimens are shown in Fig. 7. Indeed, the tensile strength of the DP specimen was lower than that of the CP specimen, however, the DPR specimen shows the highest tensile strength among the specimens tested. The highest tensile strength of DPR specimen was mainly caused by the decrease in the radii of aligned  $\text{Ni}_2\text{Si}$  nanofibers and the interdistance between them. It has been shown that an increase in tensile strength induced by work hardening is less than 60% of that brought by the nanofiber array formation in Cu–6Ni–1.4Si–0.1Ti alloys subjected to cold-rolling with 90% reduction in area [8]. The electrical conductivity of the CP and DP specimen was 25 and 44% IACS, respectively (Fig. 2), while that of the DPR specimen was 41% IACS. Consequently, the DPR specimen retained a superior combination between the tensile strength and electrical conductivity, while the tensile elongation was significantly reduced.



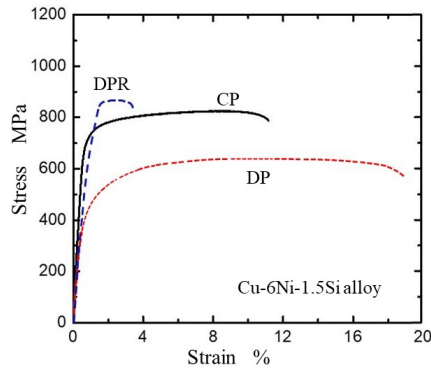


Figure 7: Stress–strain curves of the CP, DP and DPR specimens.

### 3.5 Fatigue characteristics of precipitate strengthened Cu–6Ni–1.5Si alloy

Previous studies [15], [18] indicated that the S–N plots of the CP specimen were comparable to that of the DP specimen despite a higher tensile strength for the CP specimen than that for the DP specimen, and the DPR specimen showed the highest fatigue strength among specimens tested. The fatigue limit stress at  $N = 10^7$  cycles,  $\sigma_w$ , of the DPR specimen ( $\sigma_w = 300$  MPa) was about 1.5 times of the CP ( $\sigma_w = 200$  MPa) and DP ( $\sigma_w = 195$  MPa) specimens. The ratios of  $\sigma_w$  to the tensile strength,  $\sigma_u$ , was 0.35 and 0.34 for the DP and DPR specimen, respectively, while it was 0.25 for the CP specimen.

Fig. 8(a)–(c) shows the surface morphology around an initial crack formed by cyclic stressing at  $\sigma_a = 400$  MPa. Fatigue crack in the CP specimen was initiated at GBs, followed by propagation along a favourable crystallographic slip orientation of the grain not along GBs. On the DP specimen, crack was initiated along GBs. Although the crack path just after the initiation was along GBs, the crack passed through both GBs and DP phases with further stressing. The number of cycles to create a grain-sized crack ( $l \approx 100$   $\mu\text{m}$ ) was  $3 \times 10^4$  for the CP specimen and  $7 \times 10^4$  for the DP specimen, respectively. It has been shown [14] that GB areas of the CP specimen are weakened because of PFZ formation (Fig. 4(a)). An easy GB-crack initiation of the CP specimen was attributed to weakened GB areas despite the high tensile strength compared with the DP specimen. A 100- $\mu\text{m}$  long crack in the DPR specimen was initiated after  $1 \times 10^5$  repetitions that was significantly larger than that for the CP and DP specimens. The arrays of finely distributed  $\text{Ni}_2\text{Si}$  nanofibers brought the high strength of DPR specimen and the interface of nanofibers possessed a coherency with Cu matrix [7], resulting in a drastic increase in crack initiation resistance.

Fig. 9(a) shows the crack growth curve ( $\ln l$  vs.  $N$ ) of the CP and DP specimens at  $\sigma_a = 300$  MPa. The initiation life of grain-sized crack in the CP specimen was shorter than the DP specimen (Fig. 8(a) and (b)). On the contrary, the crack growth rate was slower in the CP than the DP specimen. Accordingly, comparable S–N plots between the CP and DP specimens were attributed to the shorter life on grain-sized crack generation and longer life on crack growth of the CP specimen. Fig. 9(b) shows the comparison of crack growth curves between the DP and DPR specimens at  $\sigma_a = 400$  MPa. The slope of growth curve for the DP specimen was steeper than that for the DPR specimen, indicating an enhanced crack growth resistance in the DPR specimen.

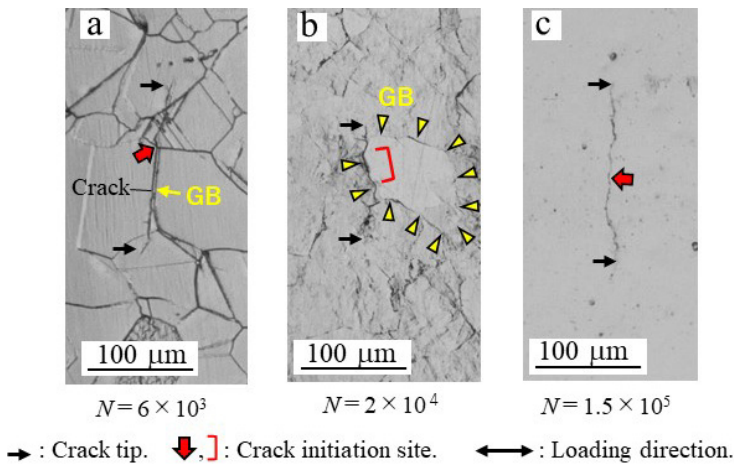


Figure 8: The surface damage around crack initiation site at  $\sigma_a = 400$  MPa. (a) The CP specimen; (b) The DP specimen; and (c) The CPR specimen.

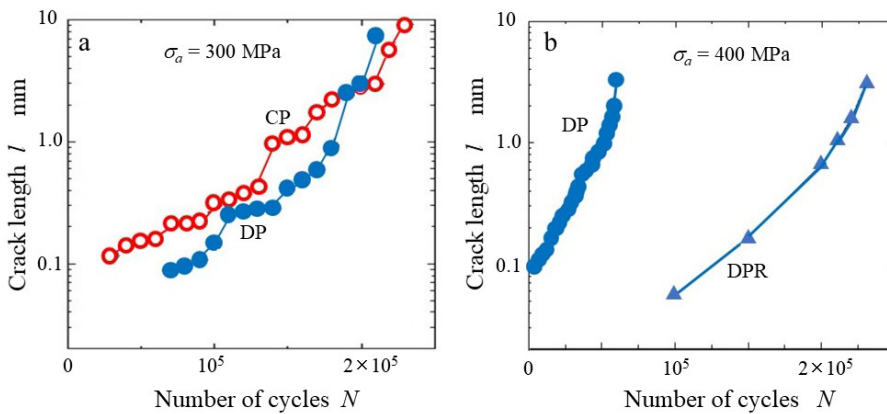


Figure 9: Crack growth curves ( $\ln l$  vs.  $N$  correlation). (a) The CP and DP specimen at  $\sigma_a = 300$  MPa; and (b) The DP and DPR specimens at  $\sigma_a = 400$  MPa.

Fig. 10(a) shows the dependency of crack growth rate (CGR,  $dl/dN$ ) on crack length  $l$  for the DPR specimen. Here, the CGR was calculated from the growth curves represented by smoothed curves which pass through the average of each set of plots. For every constant stress range, a straight line could be drawn approximately for crack length smaller than 2 mm, while the slope of the lines depended on the stress amplitude. For the range of  $\sigma_a \geq 400$  MPa, the slope is about 1, indicating that the  $dl/dN$  is proportional to  $l$ . However, the slope of line at  $\sigma_a = 350$  MPa was steeper than that for high stress ranges ( $\sigma_a \geq 400$  MPa) and was nearly equal to 2. Extended study on the  $dl/dN$  vs.  $l$  correlation of the CP and DP specimens showed that the  $dl/dN$  was nearly proportional to  $l$  at the stress range of  $\sigma_a \geq 300$  MPa.



It has been established that stress intensity factor range (SIFR,  $\Delta K$ ) is applicable to estimate the growth rate of fatigue crack propagating under the condition of small-scale yielding (a long/large crack at a comparatively low stress). The SIFR cannot estimate the growth rate of a small/short crack (e.g.,  $l < 1$  mm) [19], [20], unlike a large crack growing under a low cyclic stress. Nisitani et al. [21] and Goto and Nisitani [22] proposed eqn (1) for determining the growth rate of a mechanically small crack propagating under the large-scale yielding condition:

$$\frac{dl}{dN} = C_1 \sigma_a^n l \quad (1)$$

where  $C_1$  and  $n$  are material constants. The studies on small crack growth behaviour in various metals and alloys, such as carbon steels [21], low alloy steels [22], aluminium alloys [23], Ni-based superalloys [24], copper [25] and copper alloys [26], indicated that  $dl/dN$  of a small surface-crack in smooth specimens is determined by the term  $\sigma_a^n l$ .

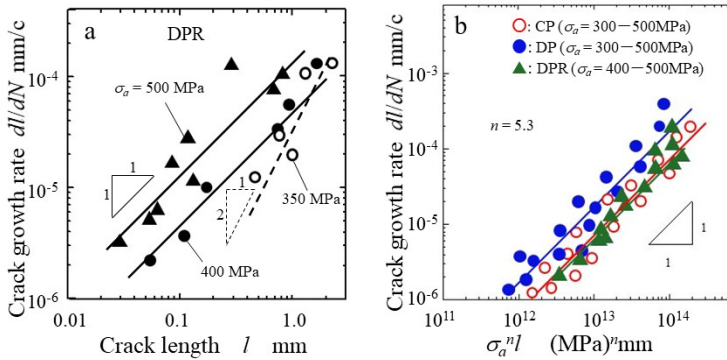


Figure 10: The crack growth data. (a) The  $dl/dN$  vs.  $l$  relationship of the DPR specimen; and (b) The  $dl/dN$  vs.  $\sigma_a^n l$  relationship of the CP, DP and DPR specimens.

Fig. 10(b) shows the growth data of a small surface-crack with the  $dl/dN$  vs.  $\sigma_a^n l$  correlation. The value of  $n$  in eqn (1) was 5.3 in all specimens. Excepting a lower stress amplitude ( $\sigma_a < 300$  MPa for the CP and DP specimens, and  $\sigma_a < 400$  MPa for the DPR specimen), the CGR could be uniquely determined by  $\sigma_a^n l$ , supporting the validity of eqn (1) for estimation of growth rate of a small crack. The crack propagation resistance of the DPR specimen was nearly equal to that of the CP specimen. Therefore, a longer fatigue life of the DPR specimen was mainly caused by an enhanced crack initiation resistance rather than crack propagation. At a low stress amplitude, the SIFR should be applicable. The slope of the  $dl/dN$  vs.  $l$  correlation at  $\sigma_a = 350$  MPa in the DPR specimen was nearly equal to 2 (Fig. 10(a)), suggesting the applicability of Paris law:  $dl/dN = C\Delta K^4$ . Bellinia et al. [27] conducted fatigue tests of Cu–Ni–Si alloy using the CT specimen. They showed the lower  $\Delta K_{th}$  and a high CGR for a low  $\Delta K$  range, followed by a well-developed Paris stage in a range of  $\Delta K > 6$  MPa·m<sup>0.5</sup>.

The fracture surfaces (1.0 mm beneath the specimen surface) of the CP, DP and DPR specimens are shown in Fig. 11. The fracture surface of the CP specimen (Fig. 11(a)) had the rough surface characterized by intergranular and transgranular facets. Such rough surface was formed as the result of crack propagation along both favourable slip planes of grains and

GBs. The transgranular fracture surface with the presence of some areas characterized by intergranular facets has been observed in Cu–Ni–Si alloy with a fine and dispersed  $\text{Ni}_2\text{Si}$  phase [27]. The fracture surface of the DP specimen was comparatively flat (Fig. 11(b)) which contrasted well with the rough fracture surface of the CP specimen. The flat surface appeared to be caused by a variety of  $\text{Ni}_2\text{Si}$  fibre orientation of DP colonies formed inside the parent grain, unlike the CP specimen with a single crystallographic slip orientation in the grain. The fracture surface of the DPR specimen is shown in Fig. 11(c). The magnified view of a highlighted area in Fig. 11(c) is likely to assist the crack growth by forming striations.

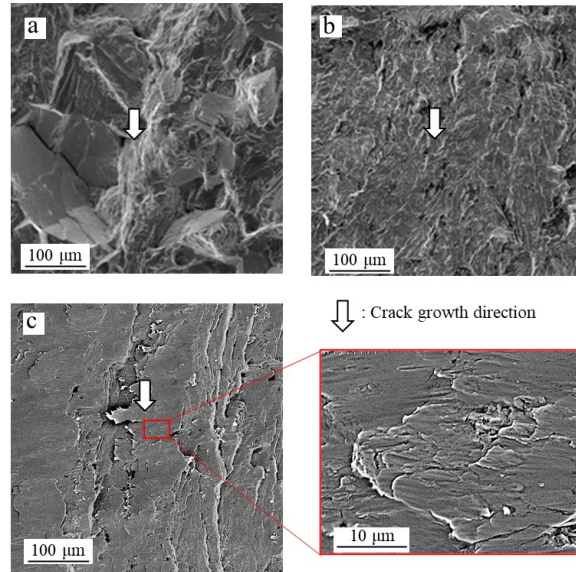


Figure 11: The fracture surface at 1.0 mm beneath the surface. (a) The CP specimen ( $\sigma_a = 300$  MPa); (b) The DP specimen ( $\sigma_a = 300$  Mpa); and (c) The DPR specimen ( $\sigma_a = 350$  MPa).

#### 4 CONCLUSIONS

The main findings of this study of the microstructure and fatigue properties on precipitate strengthened Cu–6Ni–1.5Si alloys can be summarized as follows.

1. The normal aged specimen (CP) had the matrix strengthened by disk-shaped  $\delta\text{-Ni}_2\text{Si}$  intermetallics with nano-size diameter. The microstructure of overaged specimen (DP) showed a cellular component composed of fibre-shaped  $\delta\text{-Ni}_2\text{Si}$  in the Cu matrix. The fibre-shaped  $\delta\text{-Ni}_2\text{Si}$  intermetallics were elongated in the DP specimen subjected to the cold-rolling (80%) (DPR). The diameter of  $\delta\text{-Ni}_2\text{Si}$  fibre decreased from 14 to 7 nm, while the average spacing between them decreased from 87 to 41 nm.
2. The DPR specimen showed the highest tensile strength among the specimens tested: 1.5 and 1.06 times of the DP specimen and CP specimen, respectively.
3. The fatigue limit stress at  $10^7$  cycles of the DPR specimen was 1.5 times of the CP and DP specimens. The initiation resistance of a grain-sized crack ( $l \approx 100 \mu\text{m}$ ) in the DPR specimen was drastically enhanced.

4. At the stress range of  $\sigma_a \geq 300$  MPa for CP/DP and  $\sigma_a \geq 400$  MPa for DPR specimen, the growth rate of a small crack can be determined by a term  $\sigma_a^n l$ . The value of  $n$  was 5.3 regardless of a difference in the specimens. The crack growth resistance of the DPR specimen was nearly equal to that of the CP specimen.
5. The increased tensile and fatigue strengths of the DPR specimen were attributed to a reduced spacing between  $\delta$ -Ni<sub>2</sub>Si fibres along with work hardening. Consequently, the DPR specimen was superior to the CP specimen in all of electrical conductivity, tensile strength and fatigue resistance.

#### ACKNOWLEDGEMENTS

This study was supported by a Grant-in-Aid for Scientific Research (Kiban-B) (KAKENHI: No. 18H01340) and for Encouragement of Scientists (No. 18H00244) from the Japan Society for the Promotion of Science, as well as the National Research Foundation of Korea (NRF) grant funded by the Korea government (MSIP) 2020M3D1A2098962. The authors are very grateful to the members of the Strength of Materials Laboratory of Oita University for their excellent experimental assistance. Thanks are also extended to the members of the Korea Institute of Materials Science, for the fabrication of the Cu–Ni–Si system alloys.

#### REFERENCES

- [1] Corson, M.G., Electrical conductor alloys. *Electr. World*, **89**, pp. 137–139, 1927.
- [2] Locker, S.A. & Noble, F.W., Precipitate microstructure in a Cu–Ni–Si alloy. *J. Mater. Sci.*, **29**, pp. 218–226, 1994.
- [3] Fujiwara, H., Sato, T. & Kamio, A., Effect of alloy composition on precipitation behavior in Cu–Ni–Si alloys. *J. Jpn. Inst. Metals.*, **62**, pp. 301–309, 1998.
- [4] Hu, T., Chen, J.H., Liu, J.Z., Liu, Z.R. & Wu, C.L., The crystallographic and morphological evolution of the strengthening precipitates in Cu–Ni–Si alloys. *Acta Mater.*, **61**, pp. 1210–1219, 2013.
- [5] Srivastava, V.C., Schneider, A., Ojha, V., Uhlenwinkel, S.N. & Bauckhage, K., Age-hardening characteristics of Cu–2.4 Ni–0.6 Si alloy produced by the spray forming process. *J. Mater. Process. Technol.*, **147**, pp. 174–180, 2004.
- [6] Monzen, R. & Watanabe, R., Microstructure and mechanical properties of Cu–Ni–Si alloys. *Mater. Sci. Eng. A*, **483–484**, pp. 117–119, 2008.
- [7] Favez, D., Wagnière, J.D. & Rappaz, M., Au–Fe alloy solidification and solid-state transformations. *Acta Mater.*, **58**, pp. 1016–1025, 2010.
- [8] Han, S.Z. et al., Increasing strength and conductivity of Cu alloy through abnormal plastic deformation of an intermetallic compound. *Sci. Rep.*, **6**, 30907, 2016.
- [9] Semboshi, S., Sato, S., Iwase, A. & Takasugi, T., Discontinuous precipitates in age-hardening Cu–Ni–Si alloy. *Mater. Charact.*, **115**, pp. 39–45, 2016.
- [10] Lockyer, S.A. & Noble, F.W., Fatigue of precipitate strengthened Cu–Ni–Si alloy, *Mater. Sci. Technol.*, **15**, pp. 1147–1153, 1999.
- [11] Sun, Z., Laitem, C. & Vincent, A., Dynamic embrittlement during fatigue of a Cu–Ni–Si alloy. *Mater. Sci. Eng. A*, **528**, pp. 6334–6337, 2011.
- [12] Fujii, T., Kamio, H., Sugisawa, Y., Onaka, S. & Kato, M., Cyclic softening of Cu–Ni–Si alloy single crystals under low-cycle fatigue. *Mater. Sci. Forum*, **654–656**, pp. 1287–1290, 2010.
- [13] Delbove, M., Vogt, J.-B., Bouquere, J., Soreau, T. & Primaux, F., Low cycle fatigue behavior of a precipitation hardened Cu–Ni–Si alloy. *Int. J. Fatigue*, **92**, pp. 313–320, 2016.



- [14] Goto, M., Han, S.Z., Lim, S.H., Kitamura, J., Fujimura, T., Ahn, J.-H., Yamamoto, T., Kim, S. & Lee, J., Role of microstructure on initiation and propagation of fatigue cracks in precipitate strengthened Cu–Ni–Si alloy. *Int. J. Fatigue*, **87**, pp. 15–21, 2016.
- [15] Goto, M. et al., Microstructure-dependent fatigue behavior of aged Cu-6Ni-1.5Si alloy with discontinuous/cellular precipitates. *Mater. Sci. Eng. A*, **747**, pp. 63–72, 2019.
- [16] Gholami, M. et al., Influence of grain size and precipitation hardening on high cycle fatigue performance of CuNiSi alloys. *Mater. Sci. Eng. A*, **684**, pp. 524–533, 2017.
- [17] Findik, F., Discontinuous (cellular) precipitation. *J. Mater. Sci. Lett.*, **17**, pp. 79–83, 1998.
- [18] Goto, M. et al., Simultaneous increase in electrical conductivity and fatigue strength of Cu-Ni-Si alloy by utilizing discontinuous precipitates. *Mater. Lett.*, **288**, 129353, 2021.
- [19] Miller, K.J. & de los Rios, E.G. (eds), *The Behaviour of Short Fatigue Cracks*, EGF-Pub 1, MEP, 1986.
- [20] Ravichandran, K.S., Ritchie, R.O. & Murakami, Y. (eds), *Small Fatigue Cracks: Mechanics, Mechanisms and Applications*, Elsevier, 1999.
- [21] Nisitani, H., Goto, M. & Kawagoishi, N., A small-crack growth law and its related phenomena. *Eng. Fract. Mech.*, **41**, pp. 499–513, 1992.
- [22] Goto, M. & Nisitani, H., Fatigue life prediction of heat-treated carbon steels and low alloy steels based on a small-crack growth law. *Fatigue Fract. Eng. Mater. Struct.*, **17**, pp. 171–185, 1994.
- [23] Goto, M. & Kawagoishi, N., Growth behavior and crack distribution characteristics of small surface cracks of age-hardened Al-alloy 2017-T4. *J. Society Mater. Sci. Jpn.*, **45**, pp. 675–679, 1996.
- [24] Goto, M. & Knowles, D.M., Initiation and propagation behavior of microcracks in Ni-based superalloy Udimet 720 LI. *Eng. Fract. Mech.*, **60**, pp. 1–18, 1998.
- [25] Goto, M. et al., High-cycle fatigue strength and small-crack growth behavior of ultrafine-grained copper with post-ECAP annealing. *Eng. Fract. Mech.*, **110**, pp. 218–232, 2013.
- [26] Goto, M. et al., Behaviour of small fatigue cracks in Cu-5.5Ni-1.28Si alloy round-bar specimens. *WIT Trans. Eng. Sci.*, **125**, pp. 3–13, 2019.
- [27] Bellinia, C., Brotzu, A., Di Cocco, V., Felli, F., Iacoviello, F., Pilone, D., Fatigue crack propagation mechanisms in C70250 and CuCrZr copper alloys. *Procedia Struct. Integrity*, **26**, pp. 330–335, 2020.